# A Dual-Band Ambient Energy Harvesting Rectenna Design for Wireless Power Communications

**SURAJO MUHAMMAD**[1], (Student Member, IEEE), **JUN JIAT TIANG**[1], **SEW KIN WONG**[1], **AMOR SMIDA**[2,3], (Member, IEEE), **RIDHA GHAYOULA**[3,4], **AND AMJAD IQBAL**[1], (Member, IEEE)

[1]Centre for Wireless Technology, Faculty of Engineering, Multimedia University, Cyberjaya 63100, Malaysia
[2]Department of Medical Equipment Technology, College of Applied Medical Sciences, Majmaah University, Al Majma'ah 11952, Saudi Arabia
[3]Microwave Electronics Research Laboratory, Department of Physics, Faculty of Mathematical, Physical and Natural Sciences of Tunis, Tunis El Manar University, Tunis 2092, Tunisia
[4]Department of Electrical and Computer Engineering, Laval University, Quebec City, QC G1V 0A6, Canada

Corresponding authors: Surajo Muhammad (doguwa_2002@yahoo.com) and Amjad Iqbal (aiqbal@ieee.org)

This work was supported by the TM Research and Development Malaysia under Project MMUE/190001.

**ABSTRACT** In this paper, a long-range dual-band rectenna for harvesting ambient radio frequency (RF) energy from GSM/900 and GSM/1800 is presented. Theoretical analysis of the proposed dual-band impedance matching network (IMN) is conducted using a modified Π–section matching network (MN). The RF-rectifier is integrated with a dual-band inverted-F monopole antenna. The rectenna circuit complexity is minimized by introducing a dual-band IMN, which plays a significant role in improving the harvester RF-to-dc power conversion efficiency (PCE). Measurement results of the proposed design achieved a peak RF-to-dc PCE of 12.93% and 8.0% for an input power of -30 dBm at 0.9 GHz, and 1.8 GHz, respectively. The RF harvester ambiance measurement attained an output dc voltage of 0.374 V. The circuit generates 0.747 V using a low-powered bq25504-674 evaluation module (EVM). Thus, adequate energy management of the proposed rectenna can be used to power many low-powered devices from the harvested ambient RF energy.

**INDEX TERMS** RF energy harvesting (RFEH), impedance matching network (IMN), power conversion efficiency (PCE), rectenna.

## I. INTRODUCTION

Recent advances in technology have made self-sustainable systems possible through RFEH. [1], [2]. The battery life cycle and the cost of maintenance and replacement [3] are the main challenges of the current low-powered devices [4]. The availability of electromagnetic (EM) energy from the transceiver base station (BS) and the corresponding wireless devices makes the RFEH system an additional energy source [5], [6]. The principle of EM energy transformation dates back to Tesla's experiments in the early 20th century [7], [8]. Scholars from Japan and the USA supported this in the subsequent decades [9], [10].

The antenna and RF-rectifier are the key components of the RFEH system [3]. They also referred to as rectifying

The associate editor coordinating the review of this manuscript and approving it for publication was Raghvendra Kumar Chaudhary.

antenna (rectenna) [11], [12]. The RF ambient power density picks by the RFEH antenna is considerably small. Hence, designing an RF harvester with effective RF-to-dc PCE is quite challenging [5]–[11], [13], [14]. The authors in [15] proposed a single band rectifier with a 6-stage voltage multiplier using Villard topology at 900 MHz. A rectenna with a 7-stage voltage multiplier match through a Π–MN at 900 MHz is presented in [16]. Three rectifiers are combined in [17] to form a multi-port pixel rectenna at 1800 MHz. In [18], the authors presented a dual-band rectenna operating at GSM/1800 and UMTS/2100 through a broadband antenna and a cascaded T-section MN. The authors in [19] also reported a dual-band rectifier at 915 MHz and Wi-Fi/2.45 GHz operating frequency. The authors in [20] come out with the RFEH circuit without defining the type of MN used. The rectenna uses a dual-band antenna array operating at 1800 MHz and 2.5 GHz. A dual-band rectenna for

harvesting GSM/900 and GSM/1800 RF energy is discussed in [21]. The circuits use two branches of voltage multiplier matched through a multi-section IMN. A triple-band (2 GHz, 2.5 GHz, and 3.5 GHz) differential rectenna is presented by the authors in [22]. The RF harvester receives a minimal amount of RF power density contributed by 2 GHz and 3.5 GHz operating frequencies. In [23], the authors describe a quad-band (0.95 GHz, 1.83 GHz, 2.45 GHz, and 2.62 GHz) rectifier design using a 4-stage voltage doubler suitable for high-power RFEH. The additional parasitic reported by the authors in [15], [16], [20], [21], and [23] lowered the circuit's performance besides their large electrical length. The authors in [17] and [18] reported an RF-to-dc PCE improvement but have a large antenna electrical size, besides a dc combining from multiple rectifiers in [17].

This work proposed a dual-band (900 MHz and 1800 MHz) compact rectenna with improved RF-to-dc PCE for ambient RF energy harvesting. An open literature RF spectral and the one conducted in this work show that GSM/900 and GSM/1800 frequency bands are the two dominant spectrum with higher RF power density [2], [4], [24]. Fig. 1 presents an outdoor measurement of RF power density using an Aim TTi PSA6005 6 GHz RF spectrum analyzer. These two frequency have been outlined to offer highest available RF energy that ranges from 36 nW/cm$^2$ to 84 nW/cm$^2$ [2], [4]. A compact dual-band inverted-F monopole antenna is the first design structure. The antenna is integrated with a RF-rectifier through dual-band IMN. The fabricated prototype is evaluated with low-powered power management module (PMM) using the bq25504-674 evaluation module (EVM). The major contributions of this paper focus on an improved compact rectenna RF-to-dc PCE with practical evaluation for long-distance wireless application. The proposed design can power a bq25504-674 EVM in the ambient environment. The remaining sections of the paper are organized as follows. Section II provides the RF-rectifier configuration and circuit layout. Section III outlines the RF harvester results and discussions. The antenna design parameters, geometry, and results are reported in section IV. Section V presents the performance evaluation of the fabricated layout. The conclusions are drawn in section VI.
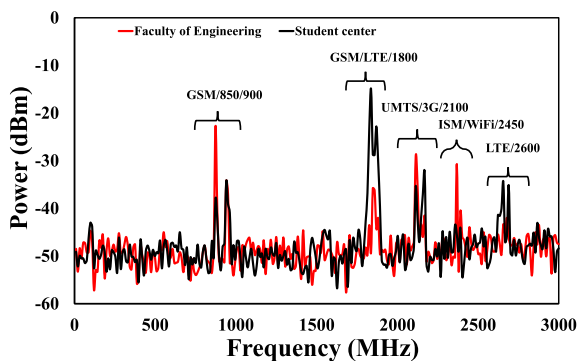


**FIGURE 1.** Measured ambient RF power density at different location (Multimedia University, Cyberjaya Campus).

## II. RECTIFIER DESIGN

Fig. 2 and Fig. 3 represent the topology of the proposed dual-band RF-rectifier. The RF-rectifier consists of a dual-band IMN, a Schottky diode, a dc-pass filter, and a load terminal ($R_L$). The circuit is designed on a 1.6 mm thick double layer FR-4 substrate with a dielectric constant of 5.4 and a loss tangent (tan$\delta$) of 0.02 connected through a 50 $\Omega$ transmission line. The MN minimizes reflection losses for the antenna RF input power [3], [11], [25], [26]. The diode plays an important role in turning the available ambient RF power into a useful dc supply [11], [27]. The dc-pass filter eliminates the fundamental and harmonic frequencies from the output signal. It also determines the performance of the output impedance and stores the available output dc supply [11], [28], [29]. $R_L$ is generally complex and frequency-dependent [30], [31]. $R_{ant}$ represents the characteristics impedance of the RF input source, with a typical input impedance of 50 $\Omega$ [32], [33].
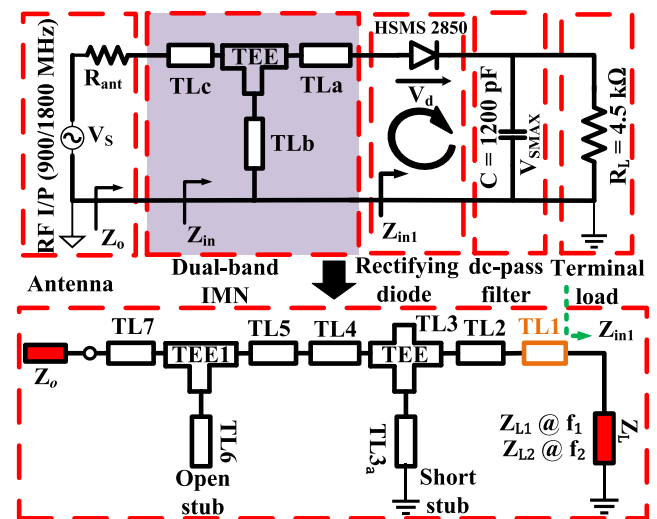


**FIGURE 2.** Rectifier detailed circuit configuration.



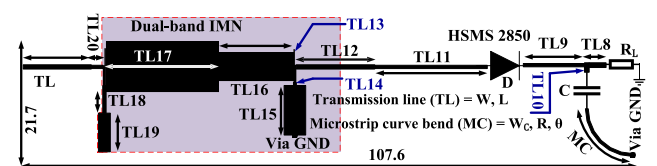**FIGURE 3.** Proposed rectifier EM model layout. The optimized circuit parameters are: L = 10.2, L8 = 4.6, L9 = 11.6, L10 = L14 = 1, L11 = 18.1, L12 = 16.7, L13 = 2.1, L15 = 10.5, L16 = 16, L17 = 19.7, L18 = 4.1, L19 = 8.2, L20 = 2.5, W = W12 = 0.9, W8 = W10 = W14 = 1, W9 = W11 = W18 = W20 = 0.7, W13 = W14 = $W_c$ = 0.6, W15 = 4.6, W16 = 6, W17 = 10.7, W19 = 2.5, R = 9.8 (All units are in mm). $\theta$ = 90$^o$, C = 1000 pF, $R_L$ = 4.5 k$\Omega$.

A source-pull simulation is an important figure to calculate the suitable value of the load terminal. This is because of the $R_L$ significance on the overall RF-to-dc PCE [34], [35]. To determine the optimal value of $R_L$, a source-pull simulation is performed across the two operating frequencies. The

results show a maximum output dc power at 4.5 kΩ load for an input power of 0 dBm. The selection of a rectifying diode to work at high frequency and low input power requires having a stable power response. For an optimal and reliable power harvester, the diode needs to handle power with minimum dissipation. Single-diode rectifiers at low input power conditions are more efficient compares to full-wave single or multi-stage rectifiers under series/shunt topology [11], [17], [32], [36], [37]. RFEH single-diode rectifiers often deliver fewer losses at low power levels, as relative to full-wave and multi-stage counterparts that introduce additional parasitic at their junction terminal. The proposed rectifier is designed on a single HSMS-2850 Schottky diode (with SOT–323 circuit layout). The diode is a promising candidate for low-power RF applications with a minimal junction capacitance of 0.18 pF and a minimum sensitive voltage of 150 mV at 0.1 mA [38], [39].

During the first stage of the design process, an advanced design system (ADS) simulates the rectifier circuit without MN, consisting only of a diode, a capacitor, and $R_L$. The dc-pass capacitor filter $C$ is also designed to block the higher-order harmonics for getting into $R_L$ at 1000 pF. $C$ is shunted with $R_L$. Upon designing $R_L$ and $C$, the diode input impedance at the two operating frequencies is computed in ADS. The rectifier input impedance is then matched to 50 Ω for proper termination with the antenna input impedance. The IMN design process is carried out through a modified Π–section MN. Hence, the IMN branch comprises an open and short-circuited transmission line stub connected through an impedance transformer TL1. To achieve an IMN with dual-band characteristics. Equation. (1) presents the complex load impedance of the rectifier at the two operating frequencies $f_1$ and $f_2$, assuming $f_2$ to be greater than $f_1$. Considering the frequency-dependency of load impedance $Z_L$, there are no direct relationships between the real load $R_{L1}$ and $R_{L2}$ and their reactance side $X_{L1}$ and $X_{L2}$. Linking of TL1 with the modified Π–section network generates dual-band impedance for transformation at $f_1$ and $f_2$.

$$Z_L = \begin{cases} Z_{L1} = R_{L1} + jX_{L1} & \text{at } f_1, \\ Z_{L2} = R_{L2} + jX_{L2} & \text{at } f_2. \end{cases} \quad (1)$$

Therefore, the TL1 free transformer converts the complex load impedance into a pair of complex conjugate impedance's $Z_{L2}$ at $f_1$ and $f_2$.

$$Z_{L2}|f_1 = (Z_{L2}|f_2)^* \quad (2)$$

By computing the electrical length ($\theta_1$) and characteristic impedance ($Z_1$) of the line, TL1 is determined by Equation. (3)–(6).

Looking from the source impedance $Z_s$, the general form of the equation is given by:

$$Z_s = \left[ R_{L1}R_{L2} + X_{L1}X_{L2} + \frac{X_{L1}+X_{L2}}{R_{L2}-R_{L2}}(R_{L1}X_{L2} - R_{L2}X_{L1}) \right]^{\frac{1}{2}} \quad (3)$$

where $Z_s = Z_o$.

$$Z_1 = \left[ R_{L1}R_{L2} + X_{L1}X_{L2} + \frac{X_{L1}+X_{L2}}{R_{L2}-R_{L1}}(R_{L1}X_{L2} - R_{L2}X_{L1}) \right]^{\frac{1}{2}} \quad (4)$$

$$Z_1 = (1+f_k)^{-1} \left\{ \arctan\left[ \frac{Z_1(R_{L1} - R_{L2})}{(R_{L1}X_{L2} - X_{L1}R_{L2})} \right] + n\pi \right\}, \quad \text{for } n = 0, 1, 3, \ldots \quad (5)$$

Hence, the length $l_1$ of the transmission line is given by:

$$l_1 = (1+f_k)^{-1}\beta_1 \left\{ \arctan\left[ \frac{Z_1(R_{L1} - R_{L2})}{(R_{L1}X_{L2} - X_{L1}R_{L2})} \right] + n\pi \right\}, \quad \text{for } n = 0, 1, 3, \ldots \quad (6)$$

where $\beta_1$ gives the phase constant of the line.

For simple analysis, $f_k$ is a frequency ratio defined by $f_2/f_1$, (and in this work, $f_k = 2$). n is carefully chosen such that $\theta_1$ is always greater than 0. The transmission line dimensions (W1, L1) and the transformed input impedance ($Z_{in1}$) are the two variables to be considered in calculating the value of n. TL1 = TL11 = (0.4 mm, 10.1 mm). A combination of TL1 and TL2 convert $Z_{in1}$ to $Z_{in}$ through open and short-circuited stubs, TL3 and TL3$_a$, respectively. The two stubs are introduced to ensure a frequency-dependent response with four degrees of freedom. The susceptance of the stubs are expressed by:

$$B_{TL}(f_i) = -Y_{TL}\cot\theta_i(f_i), \quad \text{short-circuited stub} \quad (7)$$
$$B_{TL}(f_i) = Y_{TL}\tan\theta_i(f_i), \quad \text{open-circuited stub} \quad (8)$$

where $B_{TL}$ and $Y_{TL}$ denotes the susceptance and admittance of the stub at a frequency $f_i$.

For a transmission line (TL1), the input impedance $Z_{in}$ at $f_1$ and $f_2$ can be expressed through Equation. (9)–(18):

$$Z_{in}(f_1) = Z_1\left[ \frac{(R_{L1} + jX_{L1}) + jZ_1\tan\theta_1}{Z_1 + j(R_{L1} + jX_{L1})\tan\theta_1} \right] \quad (9)$$

$$Z_{in}(f_2) = Z_1\left[ \frac{(R_{L2} + jX_{L2}) + jZ_1\tan\theta_2}{Z_1 + j(R_{L2} + jX_{L2})\tan\theta_2} \right] \quad (10)$$

Results of the transmissions TL1 to TL3 transform the impedance of $Z_{in}$ to $Z_o$ through a series of transmission lines (TL4 and TL5) and an open-circuited stub TL6 at $f_1$ and $f_2$. The electrical length of the line $\theta$ is proportional to the operating frequency $f$. Therefore, $\theta_1$, $\theta_2$, and $f_k$ can be related as $\theta_2 = f_k\theta_1$. Upon transformation of TL1, the input impedance $Z_{in1}$ at both frequencies are conjugate to each other, which can be further expressed as:

$$Z_{in1}(f_1) = Z_1\left[ \frac{R_{L1} + j(X_{L1} + Z_1\tan\theta_1)}{(Z_1 - X_{L1}\tan\theta_1) + jR_{L1}\tan\theta_1} \right] \quad (11)$$

$$Z_{in1}(f_2) = Z_1\left[ \frac{R_{L2} + j(X_{lL2} + Z_1\tan(f_k\theta_1))}{(Z_1 - X_{L1}\tan(f_k\theta_1)) + jR_{L1}\tan(f_k\theta_1)} \right] \quad (12)$$

The parameters of the transmission line are computed through the following set of equations:

$$l_i = \frac{\pi}{\beta_1 + \beta_2} \quad (13)$$

The impedance $Z_1$ of the transmission line (TL1) is derived through polynomial functions as:

$$Z_1^4 + pZ_1^3 + qZ_1^2 + rZ_1 + s = 0 \quad (14)$$

where

$$p = \frac{2f_k Z_o X_{L2}}{Z_o - R_{L2}} \quad (15)$$

$$q = \frac{Z_o R_{L2}(X_{L2}^2 - (Z_o - R_{L2})^2) - X_{L2}^2 R_o^2(1 + f_k^2)^2}{f_k^2 R_{L2}(R_{L2} - Z_o)} \quad (16)$$

$$r = \frac{2f_k Z_o^3 X_{L2}}{R_{L2} - Z_o} \quad (17)$$

$$s = \frac{Z_o^3(R_{L2}^2 + X_{L2}^2 - Z_o R_{L2})}{Z_o - R_{L2}} \quad (18)$$

$Z_2$ is determined from $Z_1$ in Equation. 14. SMA source connectors, interconnecting transmission lines, soldering lead, and SMD chip tolerance losses are among additional parasitic that are not considered during the design process. Thus, the entire RF-rectifier is fine-tuned and optimized to mitigate the impact of additional parasitic, as presented in Fig. 3.

## III. RESULTS AND DISCUSSION

Fig. 4a presents the fabricated circuits of the proposed RF-rectifier prototype. The RF-rectifier is terminated through a feed line with a 50 Ω characteristic impedance. The measurements of the proposed circuit parameters are achieved through the use of a vector network analyzer (VNA) E5062A from Agilent Technologies, a 12 GHz APSIN12G signal generator from *AnaPico* Switzerland, and a 4000 count digital multimeter (DMM) from *Sanwa*.

The measured reflection coefficient ($S_{11}$) of the proposed rectifier is obtained using the VNA, as shown in Fig. 4b.
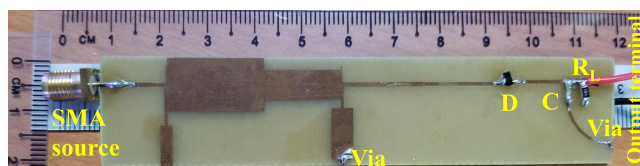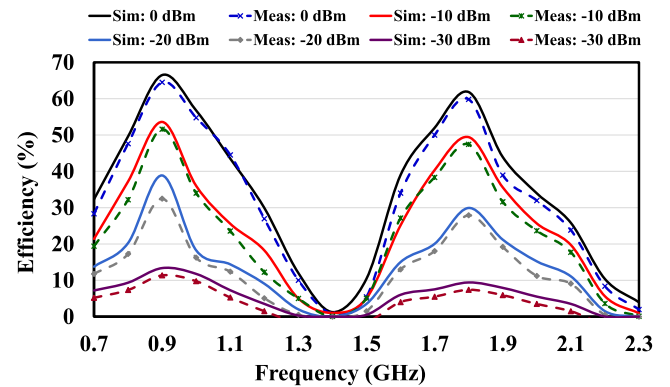


(a)
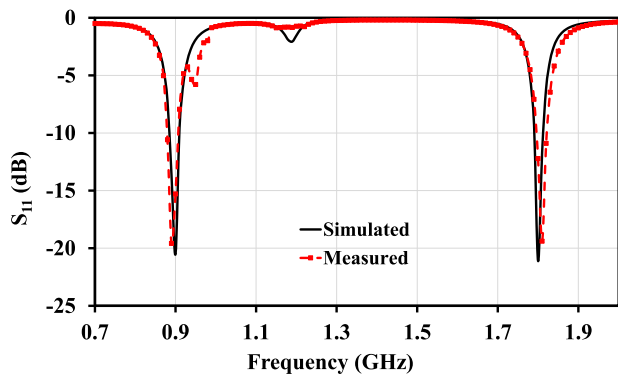


(b)

**FIGURE 4.** Proposed rectifier: (a) Fabricated prototype (b) Simulated and measured reflection coefficient $S_{11}$.

The results show a good match between the simulated and measured with slight variation from the two data. The result is achieved after a series of prototype fabrication to mitigate the effects of SMA connector loss, interconnecting, and soldering loss.



(a)
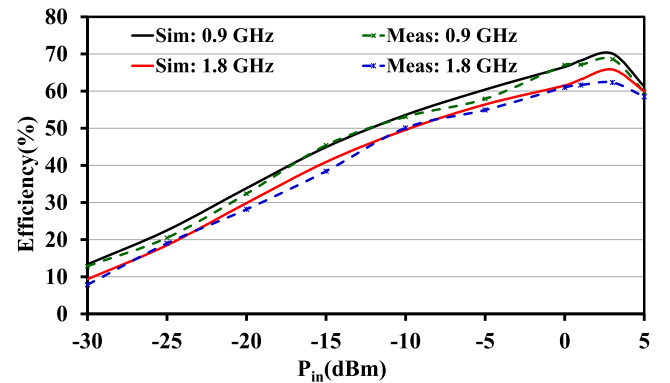


(b)

**FIGURE 5.** Proposed dual-band rectifier simulated and measured RF-to-dc PCE versus: (a) frequency (b) $P_{in}$.

Fig. 5a provides the simulated and measured RF-to-dc PCE of the proposed dual-band RF-rectifier. Simulation is carried out using a harmonic balance (HB) and a parameter sweep solver in ADS to manage the non-linear characteristics of the rectifying diode. The proposed dual-band RF-rectifier was experimentally measured through a signal generator. Different power levels (−30 dBm to 0 dBm at a span 10 dBm) were generated from the function generator between 0.7 GHz to 2.3 GHz. The input power $P_{in}$ is then swept (from −30 dBm to 5 dBm at a span of 1 dBm) at each operating frequency to evaluate the RF-rectifier RF-to-dc PCE against $P_{in}$. The output dc voltage is recorded at each sample point by the DMM across the 4.5 kΩ load terminal.

The measured output dc voltage ($V_{out}$) is used to calculate the RF-to-dc PCE of the proposed RF-rectifier, as given by:

$$\eta(\%) = P_{out}\left(\frac{1}{P_{in}}\right) \times 100\% = V_{out}^2\left(\frac{1}{R_L \times P_{in}}\right) \times 100\% \quad (19)$$

where $\eta$ represents RF-to-dc PCE and $P_{out}$ denotes output dc power of the proposed RF-rectifier. $P_{in}$ provides the

equivalent input power from the source. $V_{out}$ is the rectified dc voltage across $R_L$.

The initial RF-to-dc PCE measurement of the proposed RF-rectifier against the operating frequency were degraded. For example, the RF-rectifier realized a simulated efficiency of 70.1% and 62.3%, while the initial measurement of the fabricated prototype achieved 60.25% and 52.43%, at 0.9 GHz and 1.8 GHz for an input power of 3 dBm, respectively. This is associated with losses (from SMA source, interconnecting wires, and transmission line, soldering lead, and SMD device tolerance from the manufacturers) from the fabricated prototype. Additional parasitic attributed to the lumped elements needs to be addressed over high operating frequency because of phase shift and a distributed effects. These factors facilitate to the primary cause of parasitic which in turn lead to inaccurate results between simulation and measurements. Thus, the impacts of the parasitic at high frequencies are taken into account through components modeling from the manufacturers.

To properly handle these issues, the capacitive reactance (from C, with GCM1555C1H102FA16 part number and 0402 layout) of the initial circuit was extracted. Consequently, the effects of interconnection between the components (TL, and TL8 – TL11), Vias, and other related parasitic were addressed through transmission line optimization in ADS. After a series of optimization, the RF-rectifier was re-fabricated. The results in Fig. (4a – 5b), shows a good agreement between simulated and measured data. The proposed circuit attained a maximum measured RF-to-dc PCE of 68.62% and 62.31% at 0.9 GHz and 1.8 GHz for an input power of 3 dBm, respectively. To show the potential of the proposed rectifier for low power operation, the circuit achieved a maximum measured RF-to-dc PCE of 12.93% and 8.12% at 0.9 GHz, and 1.8 GHz for an input power of −30 dBm, respectively. Fig. 5b presents the results of the simulated and measured RF-to-dc PCE against $P_{in}$. Fig. 6 also provides the proposed dual-band RF-rectifier measurement setups for $S_{11}$ and the rectified output dc voltage.
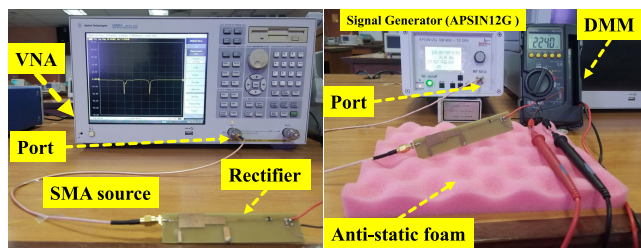
FIGURE 6. $S_{11}$ and the rectified output dc voltage measurement setups of the proposed dual-band rectifier.

To validate the optimal RF-to-dc PCE of the proposed RF-rectifier over the designed $R_L$, the circuit is simulated by varying the load terminal from 0.5 kΩ to 20 kΩ at an interval of 1 kΩ. During the measurement process, a series range of $R_L$ (from 0.5 kΩ, 1 kΩ, 1.5 kΩ…20 kΩ) is deployed at the
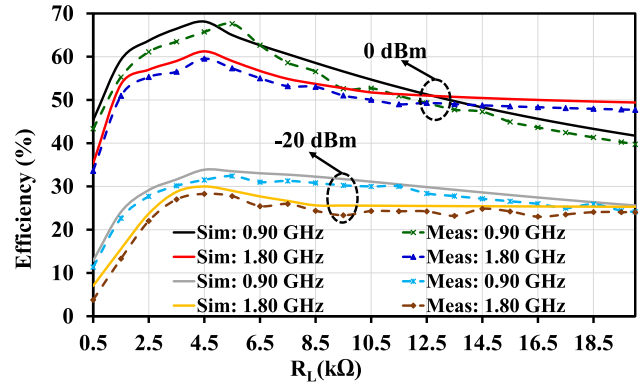
FIGURE 7. Simulated and measured RF-to-dc PCE versus load terminal ($R_L$) of the proposed dual-band rectenna circuits.

two operating frequencies to determine the peak value of $V_{out}$ for an input power of 0 dBm and −20 dBm. It is found that the circuit achieved a peak measured output dc voltage of 1.6 V and 0.9 V and a better RF-to-dc PCE of 67.0%, and 61.21% at 0.9 GHz, and 1.8 GHz for an input power of 0 dBm, respectively. During the simulation and measurement process, it was noted that a peak $V_{out}$ of (3.2 V and 2.98 V at 0.9 GHz) and (2.45 V and 2.23 V at 1.8 GHz) is recorded across the 20 kΩ load terminal. Thus, this is achieved at the detriment of the lower RF-to-dc PCE (22.35% and 21.6% at 0.9 GHz) and (12.3% and 11.58% at 1.8 GHz) at the same input power, respectively. The fabricated rectifier prototype achieved a good performance under a range of $R_L$ (from 2.5 kΩ – 8.5 kΩ) with a slight adjustment, as described in Fig. 7. A trade-off is made between the simulated and measured values of $R_L$ at 4.5 kΩ and 5 kΩ. The measured results provide an improved RF-to-dc PCE across the 5 kΩ load terminal at 0.9 GHz. This is because of the effects of parasitic and other related losses at the higher operating frequency, as previously discussed in this section. Hence, the final proposed re-fabricated RF-rectifier is analyzed using a 5 kΩ load, as shown in Fig. (4a – 7).

## IV. ANTENNA SOURCE DESIGN AND MEASUREMENT

The design of the proposed dual-band inverted-F monopole antenna is achieved from the concept of transmission line theory [5], [24], [40]. Initially, a 3 mm rectangular folded slot resonating at 0.9 GHz is added to the design. The length of the slot is computed at $\lambda/2$ (71.7 mm) of the guided wavelength. A rectangular radiator of length (18.1 mm) is loaded into the arm of the folded slot, which forms the inverted-F shape to realize the second resonant frequency at 1.8 GHz. The horizontal rectangular slot is achieved at $\lambda/4$ of the guided wavelength. The proposed antenna is excited through a 50 Ω transmission line. To improve the bandwidth of the antenna at the two operating frequencies, a 9.8 mm slit is cut from the defected ground structure. The trimmed ground plane is also realized to offer better radiation efficiency and directivity across the two operating frequencies. The antenna is also designed and printed on the same inexpensive, commercially available, and easy to fabricate FR-4 substrate. The size of
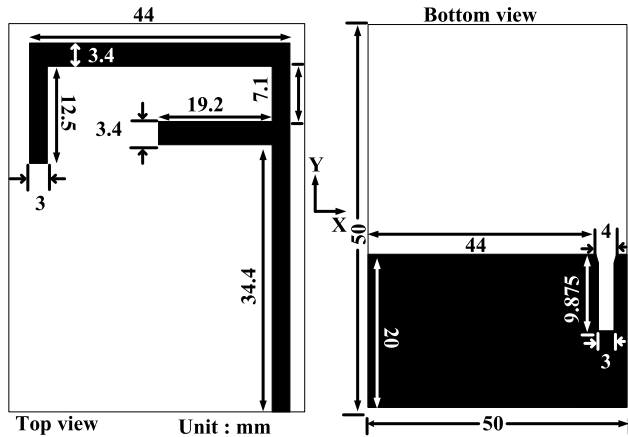
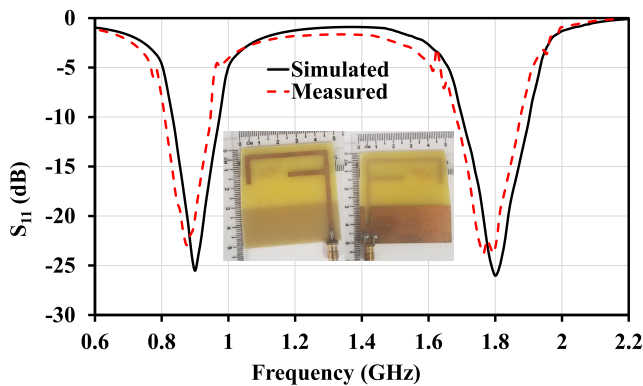**FIGURE 8.** Geometry of the proposed dual-band monopole antenna.



**FIGURE 9.** Simulated and measured $S_{11}$ of the dual-band antenna against frequency.



**FIGURE 10.** Simulated and measured radiation pattern of the proposed dual-band monopole antenna for Phi = $0^o$ and Phi = $90^o$: (a) and (b) at 0.9 GHz, (c) and (d) at 1.8 GHz respectively.

the proposed antenna is $0.30\lambda_g \times 0.30\lambda_g$. Fig. 8 presents the geometry and the optimized parameters of the antenna.

Fig. 9 presents the results of the measured and simulated $S_{11}$. The 10-dB return loss from the simulated and measured results shows that the proposed antenna covers the target operating frequency. Variable material properties possessed by the FR-4 substrate from the manufacturers, SMA source connector, and soldering losses are among the causes of the slight shift between the measured and simulated results. The antenna provides a measured bandwidth of 150 MHz (0.81 GHz – 0.96 GHZ) and 200 MHz (1.68 GHz – 1.88 GHz), at 0.875 GHz and 1.8 GHz, respectively. The dual-band antenna also realized a measured gain of 0.62 dBi and 2.36 dBi at 0.875 GHz and 1.8 GHz. The measured and simulated radiation pattern at the respective operating frequency towards *xz*-plane and *yz*-plane within the boundaries of ($\varphi = 0^o \mid 0^o < \theta < 180^0$) and ($\varphi = 90^o \mid 0^o < \theta < 180^0$) is presented in Fig. 10.

## V. OUTDOOR MEASUREMENT OF THE PROPOSED RECTENNA

The ambiance measurement of the proposed dual-band rectenna is conducted at Multimedia University, Cyberjaya
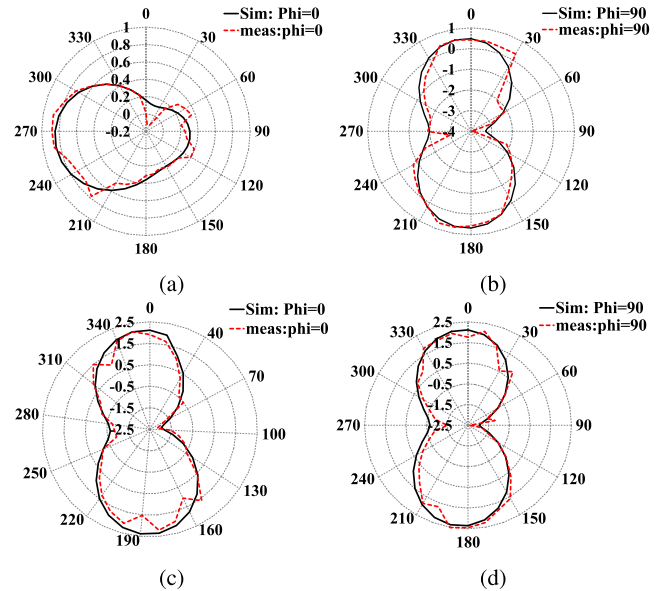
Campus. The site is located at 190 m away from the close-by cell-tower base station (BS), and all the required equipment are placed on top of a 0.5 m high rectangular table. The available RF power density in the terrain is analyzed through the spectrum analyzer. Table. 1 shows the measured available ambient power density across the two frequency bands. The signal strength from the downlink channels across the two bands is found to be the dominant one among the available ambient RF energy sources, as presented in Fig. 1, and Table. 1. The measurement around each BS is conducted at an interval of 10 m for a span of 190 m. The measurement is repeated at four (4) different locations of the BS ($90^o$ apart). The sample point from each interval is collated, and the average result is taken across each span. Hence, the results show the potential of ambient RF power for long-distance operation at GSM/900 and GSM/1800, and the proposed design focuses primarily on the two bands. The rectenna outdoor measurement achieved an output dc voltage of 0.374 V.

**TABLE 1.** Received ambient power from various public telecommunication bands.

| Band | Operating Frequency (GHz) | Received power level* (dBm) | Average received power (dBm) |
|---|---|---|---|
| GSM 900 ($M_{TX}$) | 0.88 – 0.915 | -45 – -26.5 | -27.8 |
| GSM 900 ($B_{TX}$) | 0.925 – 0.960 | -40 – -18.5 | -21.6 |
| GSM 1800 ($M_{TX}$) | 1.710 – 1.785 | -47 – -40 | -42.7 |
| GSM 1800 ($B_{TX}$) | 1.805 – 1.880 | -35 – -15 | -17.7 |

*, The site is located at a range of (10 m to 190 m for an interval of 10 m), and 1.8 m high from the close-by cell-tower BS, The measurement from the spectrum analyzer recorded at a four different location ($90^o$ apart) from the BS.

**TABLE 2.** A comparison between the proposed dual-band rectenna and other related studies from the literature.

| Ref | Dimension ($\lambda_g$) : Antenna/Rectifier (mm) | Frequency (GHz) | Peak PCE (%) : $P_{in}$ (dBm) | Power source | Substrate: Antenna/Rectifier | Diode |
|---|---|---|---|---|---|---|
| [5] | NA/0.31 × 0.05 | 0.9 | 50.2 : 2 | Ambient | NA/FR-4 (5.4) | HSMS 2850 |
| [15] | NA | 0.9 | 5 : -25 | Ambient | NA | NA |
| [16] | 0.65 × 0.52/0.60 × 0.21 | 0.9 | NA | Ambient | FR-4 (3.9) | HSMS 2850 |
| [17] | 1.10 × 0.62/3*(0.34 × 0.60) | 1.84 | 6.9 : -30 | NA | RO4003 (3.38)/RO5880 (2.2) | SMS 7630 |
| [18] | 1.80 × 0.95/1.41 × 0.62 | 1.84, 2.14 | 38.7, 34 : -18 | Ambient | RO5870 (2.33)/RO5880 (2.2) | HSMS 2852 |
| [20] | 3.45 × 1.45/0.88 × 0.57 | 1.8, 2.5 | 24 : -20 | Ambient | FR-4 (4.4) | HSMS 2850 |
| [22] | 1.70 × 1.70/1.43 × 0.61 | 2,2.5,3.5 | 53, 31, 15.5 : 7 | Ambient | FR-4 (4.4) | HSMS 285C |
| [23] | NA/1.23 × 0.51 | 0.9,1.8,2.1,2.45 | 45, 27, 28, 24 : 10 | NA | FR-4 (4.1) | HSMS 2852 |
| **This work** | **0.30 × 0.30/0.71 × 0.12** | **0.9, 1.8** | **13.2, 8.0 : -30** | **Ambient** | **FR-4 (5.4)** | **HSMS 2850** |

*$\lambda_g$, is computed at the lowest resonance frequency ($f_c$)

The multi-tone signals from the antenna source have unstable power levels because of varying ambient signals over a range of frequencies. Furthermore, the RF-rectifier impedance is characterized as a time-varying signal that needs power buffering from the PMM for maintaining a steady operation of the circuit [3], [41], [42]. As such, the proposed rectenna is further evaluated using a bq25504-674 EVM. The device uses a maximum power point tracking (MPPT) programmable module for a maximum power flow. Under a minimum quiescent current of 330 nA, the low-powered module can pick up 130 mV and 330 mV input voltage for a cold-start and a hot-start, respectively. The module requires a minimum cold-start input power of -30 dBm for a charging operation, and the integrated dc-dc boost converter can attain a practical output voltage of 3.1 V. The embedded battery management module manages the duty cycle of the output power [43], [44]. The proposed rectenna outdoor measurement setups are presented in Fig. 11. The RF harvester realized an ambiance output dc voltage of 0.747 V.

Table. 2 analyzes the relationship between the proposed rectenna and other related studies from the literature. Despite achieving compactness in [5], the circuit realized a low RF-to-dc PCE at high input power. The proposed rectenna shows better compactness with improved RF-to-dc PCE at low input power compares to the work reported by the authors in [15]– [18]. The authors in [17] does not provide the performance of the rectenna in the ambiance environment. Besides, our proposed RF harvester achieved an improved RF-dc-PCE of 13.2% and 8.0% for an input power of -30 dBm across two operating frequencies, respectively. In [20] and [22], the rectenna reported by the authors tends to have larger electrical length. Additionally, the authors in [22], [23] reported an RF harvester suitable for high-power applications. One of the unique features of the proposed dual-band rectenna in this work is the reduced circuit complexity, which lowers down the effects of parasitic. The additional circuitry in [17], [18], and [20]–[23], degrades
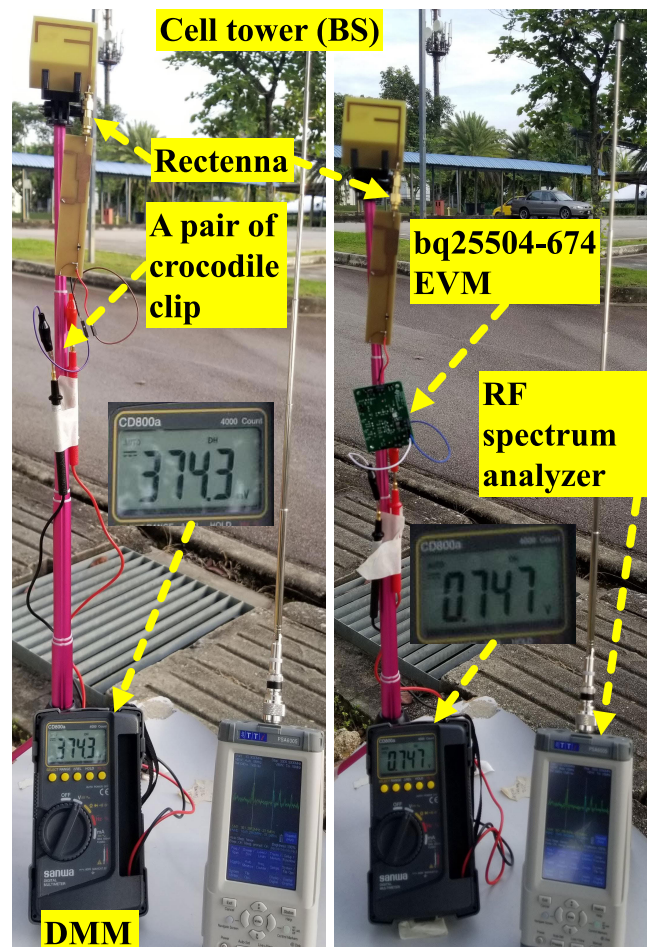


Ambiance measurement of the Rectenna.

Rectenna and EVM ambiance measurement.

**FIGURE 11.** Ambiance measurement setups of the proposed dual-band rectenna.

the overall system performance. The advantages of the proposed design in this paper compare to the other work reported in the literature comprises compactness, cheap and

easy-to-fabricate rectenna that can harvest RF signals over a long-range. The proposed dual-band RF-rectifier IMN design is derived from the closed-form equations. The IMN is realized using a modified Π-section having an extra degree of freedom. Also, the proposed rectenna shows better efficiency that drives a low power bq25504-674 EVM in an ambient environment.

## VI. CONCLUSION

This paper demonstrates the design of a dual-band rectenna for harvesting RF ambient energy from the GSM/900 and GSM/1800 band. An RF-spectral survey is conducted to assess suitable operating frequencies for RFEH systems. A unique rectenna with a dual-band inverted-F antenna and an equation driven dual-band IMN RF-rectifier has been proposed. The unique dual-band IMN of the RF-rectifier is achieved by using a modified Π-section MN with an extra degree of freedom for better impedance across the design frequencies. The rectenna outdoor performance generates 0.747 V output dc voltage using bq25504-674 EVM and 0.374 V without the low-powered module. The proposed rectenna achieved a peak RF-to-dc PCE of 12.93% at 0.9 GHz for an input power of -30 dBm. Therefore, the harvested ambient RF signals can activate several low-powered devices through appropriate energy management of the proposed rectenna.

## REFERENCES

[1] U. Muncuk, K. Alemdar, J. D. Sarode, and K. R. Chowdhury, "Multiband ambient RF energy harvesting circuit design for enabling batteryless sensors and IoT," *IEEE Internet Things J.*, vol. 5, no. 4, pp. 2700–2714, Aug. 2018.

[2] S. K. Divakaran, D. D. Krishna, and Nasimuddin, "RF energy harvesting systems: An overview and design issues," *Int. J. RF Microw. Comput.-Aided Eng.*, vol. 29, no. 1, Jan. 2019, Art. no. e21633.

[3] T. Soyata, L. Copeland, and W. Heinzelman, "RF energy harvesting for embedded systems: A survey of tradeoffs and methodology," *IEEE Circuits Syst. Mag.*, vol. 16, no. 1, pp. 22–57, 2016.

[4] Y. Luo, L. Pu, G. Wang, and Y. Zhao, "RF energy harvesting wireless communications: RF environment, device hardware and practical issues," *Sensors*, vol. 19, no. 13, p. 3010, Jul. 2019.

[5] S. Muhammad, J. J. Tiang, S. K. Wong, A. Iqbal, M. Alibakhshikenari, and E. Limiti, "Compact rectifier circuit design for harvesting GSM/900 ambient energy," *Electronics*, vol. 9, no. 10, p. 1614, Oct. 2020.

[6] S. Muhammad, J. J. Tiang, S. K. Wong, J. Nebhen, and A. Iqbal, "Design of a five-band dual-port rectenna for RF energy harvesting," *Comput., Mater. Continua*, vol. 69, no. 1, pp. 487–501, 2021. [Online]. Available: https://www.techscience.com/cmc/v69n1/42789

[7] W. Saeed, N. Shoaib, H. M. Cheema, and M. U. Khan, "RF energy harvesting for ubiquitous, zero power wireless sensors," *Int. J. Antennas Propag.*, vol. 2018, pp. 1–16, Apr. 2018.

[8] S. Nagaveni, P. Kaddi, A. Khandekar, and A. Dutta, "Resistance compression dual-band differential CMOS RF energy harvester under modulated signal excitation," *IEEE Trans. Circuits Syst. I, Reg. Papers*, vol. 67, no. 11, pp. 4053–4062, Nov. 2020.

[9] M. Cansiz, D. Altinel, and G. K. Kurt, "Efficiency in RF energy harvesting systems: A comprehensive review," *Energy*, vol. 174, pp. 292–309, May 2019.

[10] S. Shen, Y. Zhang, C.-Y. Chiu, and R. Murch, "An ambient RF energy harvesting system where the number of antenna ports is dependent on frequency," *IEEE Trans. Microw. Theory Techn.*, vol. 67, no. 9, pp. 3821–3832, Sep. 2019.

[11] C. R. Valenta and G. D. Durgin, "Harvesting wireless power: Survey of energy-harvester conversion efficiency in far-field, wireless power transfer systems," *IEEE Microw. Mag.*, vol. 15, no. 4, pp. 108–120, Jun. 2014.

[12] D. Surender, T. Khan, F. A. Talukdar, A. De, Y. M. M. Antar, and A. P. Freundorfer, "Key components of rectenna system: A comprehensive survey," *IETE J. Res.*, early access, pp. 1–27, May 2020.

[13] R. L. Rosa, P. Livreri, C. Trigona, L. D. Donato, and G. Sorbello, "Strategies and techniques for powering wireless sensor nodes through energy harvesting and wireless power transfer," *Sensors*, vol. 19, no. 12, p. 2660, 2019.

[14] D. Colaiuda, I. Ulisse, and G. Ferri, "Rectifiers' design and optimization for a dual-channel RF energy harvester," *J. Low Power Electron. Appl.*, vol. 10, no. 2, p. 11, Apr. 2020.

[15] S. Heydari Nasab, M. Asefi, L. Albasha, and N. Qaddoumi, "Investigation of RF signal energy harvesting," *Act. Passive Electron. Compon.*, vol. 2010, pp. 1–6, Dec. 2010.

[16] N. M. Din, C. K. Chakrabarty, A. B. Ismail, K. K. A. Devi, and W.-Y. Chen, "Design of RF energy harvesting system for energizing low power devices," *Prog. Electromagn. Res.*, vol. 132, pp. 49–69, Sep. 2012.

[17] S. Shen, C.-Y. Chiu, and R. D. Murch, "Multiport pixel rectenna for ambient RF energy harvesting," *IEEE Trans. Antennas Propag.*, vol. 66, no. 2, pp. 644–656, Feb. 2018.

[18] H. Sun, Y.-X. Guo, M. He, and Z. Zhong, "A dual-band rectenna using broadband Yagi antenna array for ambient RF power harvesting," *IEEE Antennas Wireless Propag. Lett.*, vol. 12, pp. 918–921, 2013.

[19] K. Niotaki, S. Kim, S. Jeong, A. Collado, A. Georgiadis, and M. M. Tentzeris, "A compact dual-band rectenna using slot-loaded dual band folded dipole antenna," *IEEE Antennas Wireless Propag. Lett.*, vol. 12, pp. 1634–1637, 2013.

[20] I. Adam, M. N. M. Yasin, H. A. Rahim, P. J. Soh, and M. F. Abdulmalek, "A compact dual-band rectenna for ambient RF energy harvesting," *Microw. Opt. Technol. Lett.*, vol. 60, no. 11, pp. 2740–2748, Nov. 2018.

[21] M. Zeng, Z. Li, A. S. Andrenko, Y. Zeng, and H.-Z. Tan, "A compact dual-band rectenna for GSM900 and GSM1800 energy harvesting," *Int. J. Antennas Propag.*, vol. 2018, pp. 1–9, Jul. 2018.

[22] S. Chandravanshi, S. S. Sarma, and M. J. Akhtar, "Design of triple band differential rectenna for RF energy harvesting," *IEEE Trans. Antennas Propag.*, vol. 66, no. 6, pp. 2716–2726, Jun. 2018.

[23] T. Skaik, "A quad-band rectifier design with improved matching bandwidth for RF energy harvesting applications," in *Proc. Int. Conf. Promising Electron. Technol. (ICPET)*, Oct. 2017, pp. 82–86.

[24] X. Lu, P. Wang, D. Niyato, D. I. Kim, and Z. Han, "Wireless networks with RF energy harvesting: A contemporary survey," *IEEE Commun. Surveys Tuts.*, vol. 17, no. 2, pp. 757–789, 2nd Quart., 2015.

[25] S. Muhammad, J. J. Tiang, S. K. Wong, A. Iqbal, A. Smida, and M. K. Azizi, "A compact dual-port multi-band rectifier circuit for RF energy harvesting," *Comput., Mater. Continua*, vol. 68, no. 1, pp. 167–184, 2021. [Online]. Available: http://www.techscience.com/cmc/v68n1/41845

[26] C. Song, Y. Huang, J. Zhou, P. Carter, S. Yuan, Q. Xu, and Z. Fei, "Matching network elimination in broadband rectennas for high-efficiency wireless power transfer and energy harvesting," *IEEE Trans. Ind. Electron.*, vol. 64, no. 5, pp. 3950–3961, May 2017.

[27] P. Li, Z. Long, and Z. Yang, "RF energy harvesting for batteryless and maintenance-free condition monitoring of railway tracks," *IEEE Internet Things J.*, vol. 8, no. 5, pp. 3512–3523, Mar. 2021.

[28] H. P. Partal, M. A. Belen, and S. Z. Partal, "Design and realization of an ultra-low power sensing RF energy harvesting module with its RF and DC sub-components," *Int. J. RF Microw. Comput.-Aided Eng.*, vol. 29, no. 1, Jan. 2019, Art. no. e21622.

[29] M. Caselli, M. Tonelli, and A. Boni, "Analysis and design of an integrated RF energy harvester for ultra low-power environments," *Int. J. Circuit Theory Appl.*, vol. 47, no. 7, pp. 1086–1104, 2019.

[30] P. Saffari, A. Basaligheh, and K. Moez, "An RF-to-DC rectifier with high efficiency over wide input power range for RF energy harvesting applications," *IEEE Trans. Circuits Syst. I, Reg. Papers*, vol. 66, no. 12, pp. 4862–4875, Dec. 2019.

[31] X. Liu and N. Ansari, "Toward green IoT: Energy solutions and key challenges," *IEEE Commun. Mag.*, vol. 57, no. 3, pp. 104–110, Mar. 2019.

[32] J. Liu and X. Y. Zhang, "Compact triple-band rectifier for ambient RF energy harvesting application," *IEEE Access*, vol. 6, pp. 19018–19024, 2018.

[33] N. Saranya and T. Kesavamurthy, "Design and performance analysis of broadband rectenna for an efficient RF energy harvesting application," *Int. J. RF Microw. Comput.-Aided Eng.*, vol. 29, no. 1, Jan. 2019, Art. no. e21628.

[34] J. Tissier and M. Latrach, "A 900/1800 MHz dual-band high-efficiency rectenna," *Microw. Opt. Technol. Lett.*, vol. 61, no. 5, pp. 1278–1283, May 2019.

[35] A. Alex-Amor, Á. Palomares-Caballero, J. Fernández-González, P. Padilla, D. Marcos, M. Sierra-Castañer, and J. Esteban, "RF energy harvesting system based on an archimedean spiral antenna for low-power sensor applications," *Sensors*, vol. 19, no. 6, p. 1318, Mar. 2019.

[36] D. Khan, S. J. Oh, S. Yeo, Y. Ryu, S. In, R. E. Rad, I. Ali, Y. G. Pu, S. S. Yoo, M. Lee, and K. C. Hwang, "A solar/triboelectric/RF hybrid energy harvesting based high efficiency wireless power receiver," *IEEE Trans. Power Electron.*, vol. 36, no. 10, pp. 11148–11162, Oct. 2021.

[37] K. T. Chandrasekaran, K. Agarwal, Nasimuddin, A. Alphones, R. Mittra, and M. F. Karim, "Compact dual-band metamaterial-based high-efficiency rectenna: An application for ambient electromagnetic energy harvesting," *IEEE Antennas Propag. Mag.*, vol. 62, no. 3, pp. 18–29, Jun. 2020.

[38] Q. Awais, Y. Jin, H. T. Chattha, M. Jamil, H. Qiang, and B. A. Khawaja, "A compact rectenna system with high conversion efficiency for wireless energy harvesting," *IEEE Access*, vol. 6, pp. 35857–35866, 2018.

[39] K. Bhatt, S. Kumar, P. Kumar, and C. C. Tripathi, "Highly efficient 2.4 and 5.8 GHz dual-band rectenna for energy harvesting applications," *IEEE Antennas Wireless Propag. Lett.*, vol. 18, no. 12, pp. 2637–2641, Dec. 2019.

[40] F. Khalid, W. Saeed, N. Shoaib, M. U. Khan, and H. M. Cheema, "Quad-band 3D rectenna array for ambient RF energy harvesting," *Int. J. Antennas Propag.*, vol. 2020, pp. 1–23, May 2020.

[41] K. K. Selim, S. Wu, and D. A. Saleeb, "RF energy scavenging with a wide-range input power level," *IEEE Access*, vol. 7, pp. 173450–173462, 2019.

[42] M. Piñuela, P. D. Mitcheson, and S. Lucyszyn, "Ambient RF energy harvesting in urban and semi-urban environments," *IEEE Trans. Microw. Theory Techn.*, vol. 61, no. 7, pp. 2715–2726, Jul. 2013.

[43] H. Tafekirt, J. Pelegri-Sebastia, A. Bouajaj, and B. M. Reda, "A sensitive triple-band rectifier for energy harvesting applications," *IEEE Access*, vol. 8, pp. 73659–73664, 2020.

[44] A. Mohan and S. Mondal, "An impedance matching strategy for micro-scale RF energy harvesting systems," *IEEE Trans. Circuits Syst. II, Exp. Briefs*, vol. 68, no. 4, pp. 1458–1462, Apr. 2021.

**SURAJO MUHAMMAD** (Student Member, IEEE) was born in 1984. He received the B.E. degree in computer engineering from Bayero University, Kano, Nigeria, and the M.E. degree in electronics and telecommunications engineering from the Universiti of Teknologi, Johor, Malaysia, in 2004 and 2014, respectively. He is currently pursuing the Ph.D. degree in RF energy harvesting with Multimedia University, Cyberjaya, Malaysia. His research interests include wideband/multiband antenna design, renewable energy systems, and RF energy harvesting. He received the TM Research and Development Scholarship for his Ph.D. research.

**JUN JIAT TIANG** received the degree in electronics engineering from Multimedia University, Malaysia, the master's degree from the University of Science, Malaysia, and the Ph.D. degree from Universiti Kebangsaan Malaysia (UKM). He worked as a Design Automation Engineer with the Chipset Structural Design Team, Intel Microelectronics (M) Sdn. Bhd., Penang, Malaysia, from September 2004 to July 2005, and an Electronics Engineer with the Global Technology Development Group, Motorola Technology Sdn. Bhd., Penang, from May 2006 to May 2007. He has vast experience while working as the Project Leader in various research grants, such as TM Research and Development, from 2017 to 2020; Research Grant, Ministry of Science, Technology and Innovation (MOSTI), from 2008 to 2010; and research grant Mini Fund, in 2016. He is currently a Senior Lecturer and a Researcher with the Faculty of Engineering, Multimedia University. His research interests include RFID, microwave circuits, antenna, and propagation. He was awarded the Gold Medal at the 23rd International Invention, Innovation, and Technology Exhibition (ITEX) 2012, Kuala Lumpur, Malaysia, in May 2012, and the Silver Medal at the Malaysian Technology Expo (MTE) 2013, Kuala Lumpur, in February 2013.

**SEW KIN WONG** received the B.E. degree (Hons.) in electronics engineering from the University Science of Malaysia (USM), in 1995, and the Master of Engineering Science and the Doctor of Philosophy degrees from the university, in 2003 and 2012, respectively, where he conducted research on radio frequency (RF) transceiver, amplifier and mixer design. Under his research contributions, a front-end RF transceiver prototype for third generation (3G) cellular communication, a power amplifier (PA), a low noise amplifier (LNA) and a down-conversion mixer integrated circuits (ICs) for ultra-wideband communication system were successfully deployed and developed. Upon graduation from his first degree in 1995, he joined Mecomb Malaysia Sdn Bhd as a Sales Engineer in charge of technical sales, presales support, and customer training for telecommunication products, ranging from simple bit error rate (BER) tester to high end synchronous digital hierarchy (SDH) test and measurement systems. He left Mecomb Malaysia Sdn Bhd, in May 2000, and joined Multimedia University as an Assistant Lecturer. He has been a Senior Lecturer with the Faculty of Engineering, Multimedia University, since 2003. His main responsibilities include conducting undergraduate and post-graduate lectures, tutorials and laboratory experiments, performing scientific research, supervising post-graduate research students, and carrying out faculty's administrative tasks. Since 2005, he has been conducting short courses and corporate trainings to engineering manufacturers, such as Agilent, Intel, Avago, Plexus, and Venture. He has conducted more than 50 courses and trainings in the area of RF/microwave and telecommunication, such as fundamental or concept, transceiver system, measurement techniques, and verifications. He is a Professional Engineer (Ir) registered under the Board of Engineers Malaysia (BEM).

**AMOR SMIDA** (Member, IEEE) received the degree in electronic baccalaureate, the M.Sc. degree in analyze and digital processing of the electronic systems, and the Ph.D. degree from the Faculty of Mathematical, Physical and Natural Sciences of Tunis, Tunis El-Manar University, Tunisia, in 2008, 2010, and 2014, respectively. From 2008 to 2014, he was a Graduate Student Researcher with the Unit of Research in High Frequency Electronic Circuits and Systems. Since August 2014, he has been an Assistant Professor with the Department of Medical Equipment Technology, College of Applied Medical Sciences, Majmaah University, Saudi Arabia. His current research interests include smart antennas, biosensors, biomedical applications, neural network applications in antennas, adaptive arrays, and microwave circuits design CST studio microwave.

**AMJAD IQBAL** (Member, IEEE) received the degree in electrical engineering from COMSATS University, Islamabad, Pakistan, in 2016, and the master's degree in electrical engineering from the Department of Electrical Engineering, CECOS University of IT and Emerging Science, Peshawar, Pakistan, in 2018. He is currently pursuing the Ph.D. degree with the Faculty of Engineering, Multimedia University, Cyberjaya, Selangor, Malaysia. He worked as a Laboratory Engineer at the Department of Electrical Engineering, CECOS University, from 2016 to 2018. His research interests include printed antennas, flexible antennas, implantable antennas, MIMO antennas, dielectric resonator antennas, and synthesis of microwave components.

• • •

**RIDHA GHAYOULA** received the Dipl. Eng. degree in electrical engineering, the M.Sc. degree in analyze and digital processing of the electronic systems, and the Ph.D. degree from the Faculty of Mathematical, Physical and Natural Sciences of Tunis, Tunis El-Manar University, Tunisia, in 2002, 2005, and 2008, respectively.

From 2004 to 2012, he was a Graduate Student Researcher with the Unit of Research in High Frequency Electronic Circuits and Systems. Since August 2009, he has been an Assistant Professor with the Electrical Engineering Department, Higher Institute of Computer Science of El Manar, Tunisia, and an Associate Professor from 2014 to 2015. Since May 2012, he has been a Postdoctoral Fellow with the LRTS, Department of Electrical and Computer Engineering, Laval University, Quebec City, Canada. He has worked on several industrial experiences in Canada, such as an FPGA Designer with Aerostar Research and Development in 2014; Doric Lenses Inc., in 2017; Telops Inc., in 2018; and M2S Electronics Canada, in 2019. He has published more than 80 journals and conference papers on smart antennas and embedded systems. His current interests include software engineering, FPGA, softcore processor, modeling and simulation, TDOA, DOA, phased arrays, smart antennas, direction finding, radio-communication systems, neural network applications in antennas, adaptive arrays, and microwave circuits design. He participated in several industrial projects in North America for seven years in the embedded field, real time, LidAR and FPGA, dual optogenetic stimulation with a laser diode fiber light source, hyperspectral IR cameras, DE-8209 ORKAN - UP15 (C0069A), HVAC application: TNG15-TX070, and HVAC application: DE-8209 TOUCH18 WiFi-TX120.